ISSN 1063-7834, Physics of the Solid State, 2018, Vol. 60, No. 12, pp. 2491–2497. © Pleiades Publishing, Ltd., 2018.
Original Russian Text © G.V. Bazuev, T.I. Chupakhina, A.V. Korolev, 2018, published in Fizika Tverdogo Tela, 2018, Vol. 60, No. 12, pp. 2389–2395.

MAGNETISM

Effect of Cobalt on the Crystal Structure and Magnetism of Electron-Doped $Sr_{0.8}Ce_{0.2}MnO_3$ Oxide

G. V. Bazuev[a, *], T. I. Chupakhina[a], and A. V. Korolev[b]

[a] *Institute of Solid State Chemistry, Ural Branch, Russian Academy of Sciences, Yekaterinburg, 620990 Russia*

[b] *Mikheev Institute of Metal Physics, Ural Branch, Russian Academy of Sciences, Yekaterinburg, 620108 Russia*

**e-mail: bazuev@ihim.uran.ru*

Received June 14, 2018

Abstract—The $Sr_{0.8}Ce_{0.2}Mn_{1-y}Co_yO_{3-\delta}$ ($y = 0.2$, 0.3, 0.4, 0.5, and 0.6) complex oxides with the perovskite structure obtained from simple oxides by the solid–state reaction technique have been examined using structural analysis and magnetic measurements. Substitution of Co for Mn in the dilute $Sr_{0.8}Ce_{0.2}MnO_3$ antiferromagnet with a Néel temperature of $T_N = 210$ K leads to a decrease in the degree of tetragonal distortion of the crystal structure and transition to the cubic cell. The degeneracy of the antiferromagnetic interaction ($T_N = 138$ K at $y = 0.2$) observed at the first stage of the substitution of Co for Mn changes for its gradual enhancement with an increase in the magnetic transformation temperature up to 239 K at $y = 0.6$. An increase in the Co content weakens the competition between the ferromagnetic and antiferromagnetic couplings and reduces the temperature of the transition to the spin-glass-like state. The magnetic inhomogeneity and formation of Co^{2+}–Mn^{4+} ferromagnetic clusters in $Sr_{0.8}Ce_{0.2}Mn_{0.4}Co_{0.6}O_{2.69}$ at 140 K have been observed.

DOI: 10.1134/S1063783418120089

1. INTRODUCTION

Manganites and cobaltites of alkaline- and rare-earth elements with the perovskite structure attract attention of researchers due to their interesting physical and chemical properties important for application. In particular, the interest in $Ln_{1-x}A_xMnO_3$ (Ln is the rare-earth element and A is the alkaline-earth element) manganites is due to the colossal magnetoresistive effect caused by the optimal balance between spin, charge, and orbital orderings [1, 2]. The $SrCoO_3$ cobaltite is a ferromagnet with a Curie temperature of $T_C = 270$–300 K and metallic conductivity [3], while the substituted cobaltite $La_{1-x}Sr_xCoO_3$ has a complex phase diagram with the antiferromagnetism and insulator behavior at the low Sr concentrations and ferromagnetism and conductive properties at the high Sr concentrations.

In [4–6], the effect of substitution of Co for Mn in the $La_{1-x}A_xMn_{1-y}Co_yO_3$ (A = Ca, Sr) complex oxides with the hole conductivity was studied. It was established that an increase in the Co content leads to the weakening of the ferromagnetic ordering and formation of the spin-glass-like state of the cluster type inside the ferromagnetic state. In particular, the magnetism of the $La_{1.25}Sr_{0.75}MnCoO_6$ perovskite was identified using two transformations: a ferromagnetic transition at T_C (217 K) and a frequency-dependent transition at $T_g < 100$ K [6]. The high T_C value is determined by the local T_C values of weakly fluctuating clusters based on the valence combination of Co^{2+}–Mn^{4+}, while the low spontaneous moment at 2 K results from their low content.

It is interesting to investigate the effect of cobalt on the structure and properties of electron-doped manganites, including $A_{1-x}Ce^{4+x}MnO_3$ (A is Sr or Ca) solid solutions (SSs) [7–9], which are considered to be potential cathode materials for solid-state fuel cells [10]. The Ce-substituted $A_{1-x}Ce_x^{4+}CoO_3$ cobaltites are attractive for studying the influence of a heterovalent substitution on the Curie temperature and conductivity [11, 12].

Substitution of high-valence Ce^{4+} cations for strontium in $SrMnO_3$ and $SrCoO_3$ significantly affects their structural and charge characteristics and magnetic and transport properties. As is known [13], $SrMnO_3$ prepared under normal conditions has a hexagonal structure and is an antiferromagnet with a Néel temperature of $T_N = 278$ K. Embedding of high-valence Ce^{4+} cations in the Sr sites first (at $x = 0.01$–0.05) stabilizes the $Sr_{1-x}Ce_xMnO_3$ cubic structure and, at $0.1 < x \leq 0.3$, the tetragonally distorted perovskite structure

(sp. gr. *I*4/*mcm*). In this case, the corresponding number of Mn^{4+} cations are reduced to Mn^{3+} ones, which leads to a strong distortion of MnO_6 octahedra and an increase in the parameter *a* and unit cell volume. The parameter *c* in $Sr_{1-x}Ce_xMnO_3$ first increases, attaining its maximum value at $x = 0.15$, and then decreases [14].

The magnetic and electrical properties of these SSs depend, to a great extent, on the *x* value. The $Sr_{0.9}Ce_{0.1}MnO_3$ SS is a *C*-type antiferromagnet with $T_N = 290$ K, which passes from the metallic to semiconductor state at 315 K. The magnetic behavior of $Sr_{1-x}Ce_xMnO_3$ at $0.1 < x < 0.3$ is caused by the strong competition between the double exchange and superexchange couplings [9], which results in the absence of a magnetically ordered state in this system and the dominance of the cluster or spin-glass-like state at low temperatures (below 20 K). The temperature dependence of the magnetic susceptibility of the $Sr_{0.8}Ce_{0.2}MnO_3$ sample has a broad maximum at 150–300 K, which is interpreted in the framework of a concept of dilute antiferromagnetism with $T_N = 210$ K. According to [8], in the paramagnetic region ($x \geq 0.2$), the ferromagnetic clusters form.

The solid solutions with $x = 0.25$ and 0.35 [9] are characterized by the negative magnetoresistive effect based on the charge ordering, which occurs near 110 K.

Zhang et al. [15] reported on the synthesis, structure, and conductive properties of the $Sr_{0.8}Ce_{0.2}Mn_{0.8}Co_{0.2}O_3$ complex oxide. In contrast to $Sr_{0.8}Ce_{0.2}MnO_3$, the octahedra in the Co-containing compound structure are regular, which is due to the absence of Jahn–Teller Mn^{3+} cations. Embedding of cobalt to the Mn sites reduces the electrical conductivity. The electrochemical characteristics of the Co-doped $Sr_{0.8}Ce_{0.2}MnO_3$ compound as a cathode material were described in [10].

The crystal structure of the $Sr_{1-x}Ce_xCoO_{3-\delta}$ compound obtained under high-pressure [11] remains cubic up to $x = 0.4$. When the synthesis is performed in sealed ampoules, the cubic phase concentration range is limited to $0 < x < 0.15$ [12]. This SS has a crystal structure of the high-temperature $SrCoO_{3-x}$ modification and is characterized by the high oxygen exchange and electrical conductivity. The oxygen deficiency in the $Sr_{1-y}Ce_yCoO_{3-\delta}$ compound increases with temperature and decreases with increasing partial pressure of oxygen and Ce concentration.

In this work, we present the results of investigations of the structural characteristics and magnetic properties of the double-substitution $Sr_{0.8}Ce_{0.2}Mn_{1-y}Co_yO_{3-\delta}$ SSs in a wide concentration range (*y* is 0.2, 0.3, 0.4, 0.5, and 0.6). In our previous study [16] of two samples in this series ($y = 0.3$ and 0.4), we showed that embedding of cobalt to the manganese sites in $Sr_{0.8}Ce_{0.2}Mn_{1-y}Co_yO_{3-\delta}$ is interesting in terms of the crystal structure evolution and competition between the antiferromagnetic and ferromagnetic couplings. In [17], we analyzed the Ce, Mn, and Co oxidation states in the $Sr_{1-x}Ce_xMn_{1-y}Co_yO_{3-\delta}$ SSs using X-ray absorption spectroscopy and magnetic measurements.

2. EXPERIMENTAL

The $Sr_{0.8}Ce_{0.2}Mn_{1-y}Co_yO_{3-\delta}$ samples were synthesized by the solid-phase reactions from CeO_2, MnO_2, Co_3O_4, and $SrCO_3$ simple oxides containing no lower than 99.95% of the basic substance. The stoichiometric mixtures of these oxides and strontium carbonate were thoroughly grinded, pressed at a pressure of 3000 kg/cm^2, and sintered at a temperature increased with a step of 100°C with intermediate grinding each 10 h. The calcined reaction products were cooled in a furnace to room temperature. The initial annealing temperature was 950°C and the final temperature was 1350°C. The presence of impurities in the products was monitored by X-ray diffraction on a Shimadzu XRD-7000S diffractometer using the PDF 2 database (ICDD, USA, Release 2009). The processing of diffraction patterns and refinement of the crystallochemical parameters were performed by a Rietveld full-profile analysis using the FULLPROF 2016 program.

The oxygen content in the samples was analyzed by the weight loss upon calcination in the H_2 flow at 950°C for four hours. The oxygen index in the initial samples was calculated taking into account the fact that during the reaction cobalt is reduced to the metallic state and the residual oxygen is bound to divalent manganese, trivalent cerium, and SrO.

The magnetic measurements were performed at the Center of Collective Use of the Mikheev Institute of Metal Physics, Ural Branch, Russian Academy of Sciences on a QD MPMS-XL-5 SQUID magnetometer in the temperature range of 2–300 K in magnetic fields of 0.5 and 5.0 kOe (dc susceptibility). The measurements were performed upon cooling the samples in measured (*FC* data) and zero (*ZFC* data) magnetic fields. Using the dynamic magnetic susceptibility (ac susceptibility) measuring technique, the real (χ') and imaginary (χ'') susceptibility components were determined at ac magnetic field amplitudes of up to 4 Oe and a frequency of 80 Hz. The magnetization curves and magnetic hysteresis loops were obtained at 2 K on the samples cooled in zero magnetic field according to the following scheme: first, the magnetization curve was measured in a magnetic field increased from 0 to +50 kOe and then the hysteresis loops were measured upon field variation from +50 to −50 kOe and from −50 to +50 kOe.

3. RESULTS AND DISCUSSION

3.1. Structural Characteristics of the $Sr_{0.8}Ce_{0.2}Mn_{1-y}Co_yO_{3-\delta}$ ($y = 0.2, 0.3, 0.4, 0.5$, and 0.6) SS

According to the X-ray data, all the samples with y values between 0.2–0.6 are single-phase. The composition with $y = 0.7$ contains, along with the main phase, CeO_2. The $Sr_{0.8}Ce_{0.2}MnO_3$ crystal structure parameters obtained by us are almost consistent with those reported in [8]. Table 1 gives the parameters a and c of the $Sr_{0.8}Ce_{0.2}Mn_{1-y}Co_yO_3$ ($y = 0$–0.6) SS and oxygen contents the samples. It was established that the SSs with $y = 0.2$ and 0.3, similar to $Sr_{0.8}Ce_{0.2}MnO_3$, are tetragonal (sp. gr. *I*4/*mcm*). The samples with $y \geq 0.4$ have a cubic cell (sp. gr. *Pm*3*m*). Thus, the SSs with $y \geq 0.4$ undergo the phase transition from the tetragonal to cubic syngony stable in the SSs with $y = 0.5$ and 0.6. The decrease in the oxygen content in the SS upon substitution of Co for Mn is indicative of the formation of oxygen-deficient samples, which is quite natural and agrees with the $Sr_{0.9}Ce_{0.1}CoO_{3.69}$ cobaltite composition [12].

Figure 1 shows dependences of the parameters a and c and volume V of the $Sr_{0.8}Ce_{0.2}Mn_{1-y}Co_yO_{3-\delta}$ SS unit cell on the y value. The a, c, and V values for the SSs with $y = 0$, 0.2, and 0.3 in Fig. 1 are presented for comparison for a simple perovskite cell. The averaged parameter V_0 for the tetragonal SSs was calculated using the formula $V_0 = a^2c/V$. It can be seen that with an increase in the degree of substitution of Co for Mn, the crystal lattice parameters significantly change. Embedding of Co in the oxygen octahedron leads, first of all, to a sharp decrease in the parameter c, which is caused by a decrease in the number of Mn^{3+} cations. In the range from 0 to 0.3, the parameter a decreases weaker.

The unit cell volume of the SS with a tetragonal structure in this y range also decreases with increasing cobalt content. At $y > 0.3$ and in the cubic SSs, the parameter a and volume V increase. The solid solution with the maximum Co content ($Sr_{0.8}Ce_{0.2}Mn_{0.4}Co_{0.6}O_{2.69}$) has the parameter a (3.841 Å) similar to the parameter of $Sr_{0.9}Ce_{0.1}CoO_{2.74}$ ($a = 3.843$ Å [12]).

3.2. Magnetic Properties of the $Sr_{0.8}Ce_{0.2}Mn_{1-y}Co_yO_{3-\delta}$ SS

The measured magnetic characteristics of the $Sr_{0.8}Ce_{0.2}Mn_{1-y}Co_yO_{3-\delta}$ SS in the range of 2–300 K are shown in Figs. 2–5. The temperature dependences of the magnetic susceptibility χ for all the investigated samples at $H = 5$ kOe have two anomalies (Figs. 2 and 3) and demonstrate a decrease in x with the increasing Co content. The high-temperature T_{max1} anomalies at all the y values correspond to the transition from the paramagnetic to some new magnetic state. The fact that the FC magnetic susceptibility does not tend to a sharp increase at temperatures below T_{max1} allows us to conclude that there is no ferromagnetic ordering in all the investigated SSs. Below these maxima, the FC and ZFC curves start diverging; the discrepancy between them sharply increases at T_{max2} (at 20–40 K). The discrepancy between the FC and ZFC curves below the magnetic transformation point T_{max1} is typical of all the Co-containing samples. The measurements in magnetic fields of 0.5 and 5 kOe coincide, except for the SS with $y = 0.6$. It follows from Fig. 4 that the temperature dependence of χ for $Sr_{0.8}Ce_{0.2}Mn_{0.4}Co_{0.6}O_{2.69}$ measured in a field of $H = 0.5$ kOe contains one more anomaly accompanied by a sharp divergence of the ZFC and FC curves. This anomaly accompanied by small maxima in the ZFC curves at 136 K in a field of 500 Oe is especially pronounced and shifted to 142 K when measured in a magnetic field of 100 Oe (inset in Fig. 4).

Table 1. Structural parameters and oxygen content in the $Sr_{0.8}Ce_{0.2}Mn_{1-y}Co_yO_{3-\delta}$ solid solutions

y	Space group	a, Å	c, Å	V, Å^3	δ
0 [8]	*i*4/*mcm*	5.4013(1)	7.7481(1)	225.95	0
0.2	*I*4/*mcm*	5.3962(1)	7.6674(1)	223.22(1)	0.04
0.3	*I*4/*mcm*	5.3953(1)	7.6487(1)	222.64(1)	0.06
0.4	*Pm*3*m*	3.8222(1)		55.83	0.12
0.5	*Pm*3*m*	3.8292(1)		56.15	0.25
0.6	*Pm*3*m*	3.8406(1)		56.65	0.31

At the minimal substitution of Co for Mn ($y = 0.2$), the SS is characterized by a weaker broad maximum in the $\chi(T)$ dependence in the range of 100–160 K (Fig. 2) as compared with $Sr_{0.8}Ce_{0.2}MnO_3$ [8]. The temperature dependence of the magnetic susceptibil-

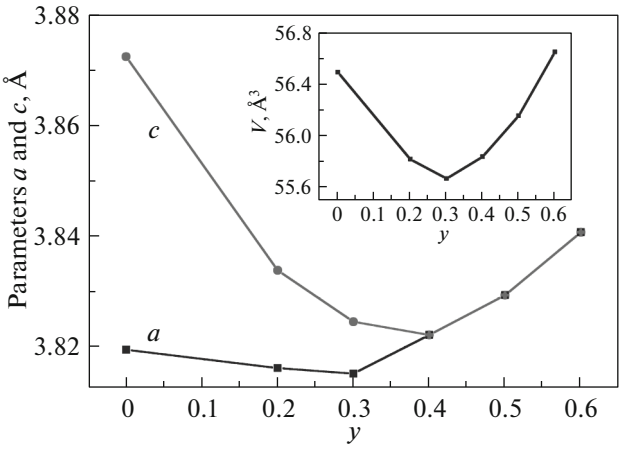

Fig. 1. Dependence of the parameters a and c and volume V (inset) for $Sr_{0.8}Ce_{0.2}Mn_{1-y}Co_yO_{3-\delta}$ on the cobalt content.

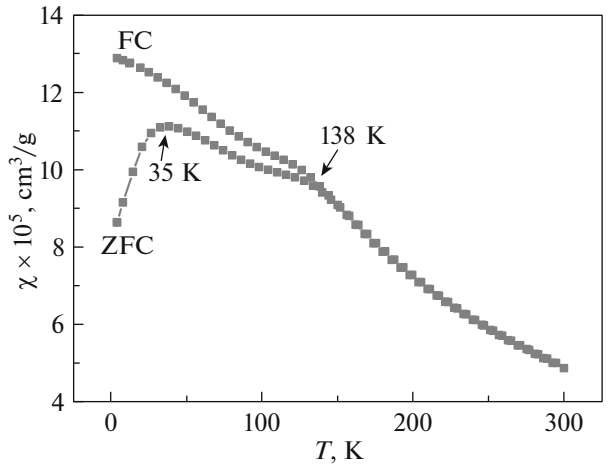

Fig. 2. Temperature dependence of magnetic susceptibility χ for $Sr_{0.8}Ce_{0.2}Mn_{0.8}Co_{0.2}O_{2.96}$ in a magnetic field of 5 kOe.

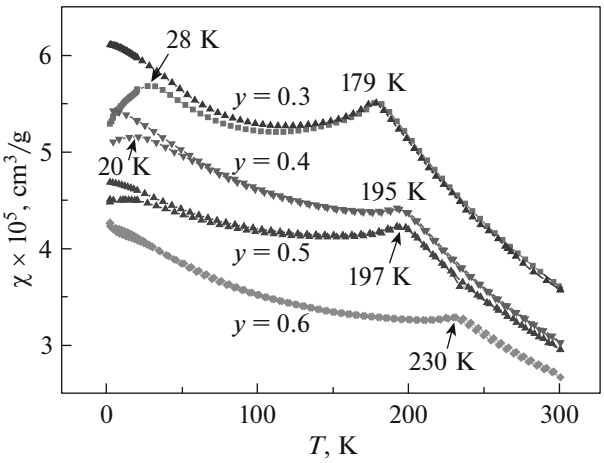

Fig. 3. Temperature dependence of magnetic susceptibility χ for $Sr_{0.8}Ce_{0.2}Mn_{1-y}Co_yO_{3-\delta}$ (y = 0.3–0.6) in a magnetic field of 5 kOe.

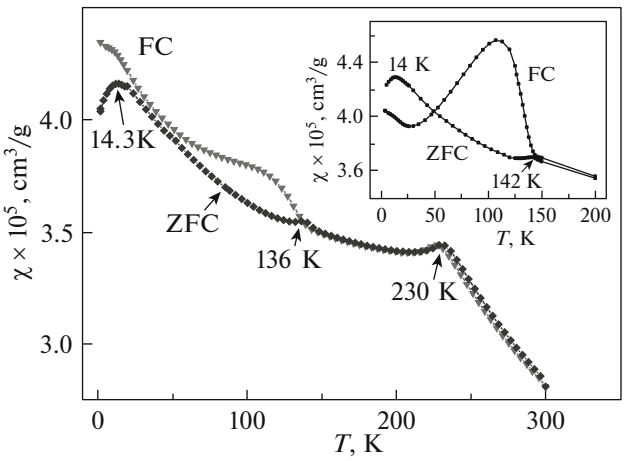

Fig. 4. Temperature dependence of magnetic susceptibility χ for $Sr_{0.8}Ce_{0.2}Mn_{0.4}Co_{0.6}O_{2.70}$ in magnetic fields of 0.5 and 0.1 (inset) kOe.

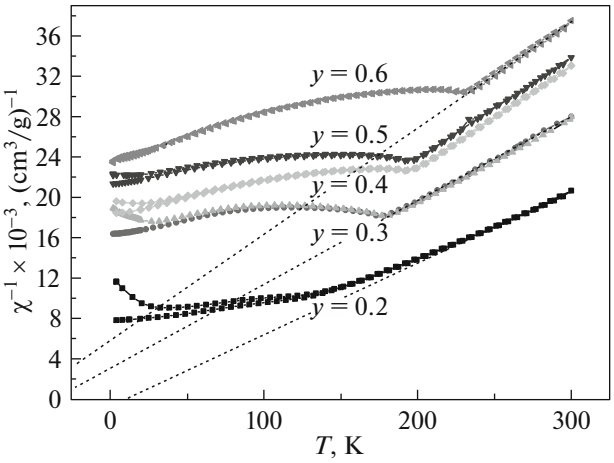

Fig. 5. Temperature dependence of reciprocal magnetic susceptibility $\chi^{-1}(T)$ for $Sr_{0.8}Ce_{0.2}Mn_{1-y}Co_yO_{3-\delta}$ (y = 0.2–0.6) in a magnetic field of 5 kOe.

ity below 138 K reveals a discrepancy between the ZFC and FC curves and the $\chi(T)$ curve has no kink typical of the AFM transition related to a decrease in the magnetic susceptibility. At the same time, the $\chi^{-1}(T)$ dependence (Fig. 5) obeys the Curie–Weiss law far above T_{max1} (138 K) and has the positive Θ constant in the range of 250–400 K, as in $Sr_{0.8}Ce_{0.2}MnO_3$ [8].

In the SSs with the higher cobalt content, the maximum at T_{max1} becomes more clear and shifts towards higher temperatures to 179, 195, 197, and 230 K at y = 0.3, 0.4, 0.5, and 0.6, respectively (Fig. 3). At y = 0.3, 0.4, and 0.5, upon further cooling in the range of 75–100 K, the magnetic susceptibility slightly increases, which is accompanied by the divergence of the FC and ZFC curves. At 28 K (y = 0.3), 20 K (y = 0.4), and 15 K (y = 0.5), the maxima in the ZFC dependences are fixed. It can be seen in Fig. 5 that at high temperatures the magnetic susceptibility of SSs with x values of 0.3, 0.4, 0.5, and 0.6 obeys the Curie–Weiss law

$$\chi = C/(T - \Theta),$$

where C is the Curie constant (cm^3) and Θ is the Curie–Weiss constant (K). The negative Θ values are indicative of the preferred antiferromagnetic couplings. The solid solution with x = 0.2 is characterized, similar to $Sr_{0.8}Ce_{0.2}MnO_3$, by the positive Θ constant (Table 2).

The magnetization curves at 2 K (Fig. 6) contain narrow hysteresis loops without saturation traces in a magnetic field of 50 kOe with a residual magnetization

Table 2. Magnetic properties of the $Sr_{0.8}Ce_{0.2}Mn_{1-y}Co_yO_{3-\delta}$ solid solutions

y	Θ, K	C, emu K/mol	T_g K	T_N, K
0.2	11	2.83	35	138
0.3	−34.7	2.42	28	179
0.4	−39.4	2.0	20	195
0.5	−35.6	1.96	16	197
0.6	−80	1.98	12	230

of up to 0.02 emu/g and coercivity B of up to 350 Oe. Taking these data into account, the low-temperature anomalies for the $Sr_{0.8}Ce_{0.2}Mn_{1-y}Co_yO_{3-\delta}$ SSs at 20–34, as in the case of $Sr_{0.8}Ce_{0.2}MnO_3$ [9], should be attributed to the transitions to the spin-glass-like state.

According to the ac susceptibility measured for a number of samples (Fig. 7), the $\chi'(T)$ curves exhibit anomalies at temperatures similar to T_{max1} and T_{max2} recorded during the dc susceptibility measurements.

Tables 2 and 3 give the magnetic characteristics of all the investigated samples. The data on the sample with $y = 0.2$ were obtained from the $\chi^{-1}(T)$ dependence in the range of 250–400 K [16]. According to the RAS and XANES data from [15, 17], cerium in these SSs has the form of Ce^{4+} cations; therefore, the total magnetic moment corresponds to cobalt and manganese cations. The Mn and Co valence and spin states in $Sr_{0.8}Ce_{0.2}Mn_{1-y}Co_yO_{3-\delta}$ ($y = 0.2$–0.6) were calculated taking into account the data on the oxygen nonstoichiometry of the samples (Table 1) and the experimental effective magnetic moments. In the calculations, we used the following configurations of cations in the octahedral environment: Mn^{4+} ($t_{2g}^3e_g^0$, $S = 3/2$), Mn^{3+} ($t_{2g}^3e_g^1$, $S = 2$), Co^{2+} ($t_{2g}^5e_g^2$, $S = 3/2$), and Co^{3+} ($t_{2g}^4e_g^2$, $S = 2$ – the high-spin state). In addition, the spin–orbit contribution to the Co^{2+} effective magnetic moment was taken into account.

It follows from the data given in Table 2 that the experimental effective magnetic moment μ_{exp} ($4.76\mu_B$) for the $Sr_{0.8}Ce_{0.2}Mn_{0.8}Co_{0.2}O_3$ compound is much higher than the μ_{calc} value calculated assuming manganese to have the form of Mn^{4+} cations and cobalt to have the Co^{2+} form. Meanwhile, as was shown in study [15] by the XANES technique, Mn in $Sr_{0.8}Ce_{0.2}Mn_{0.8}Co_{0.2}O_3$ has the higher valence than in $Sr_{0.8}Ce_{0.2}MnO_3$. This means that the larger Mn fraction in this SS has the form of Mn^{4+} cations and Co is in the form of Co^{2+} cations. This conclusion agrees with the results of investigations of other Mn and Co complex oxides, including those with the perovskite [6] and spinel structures [18], where the stable

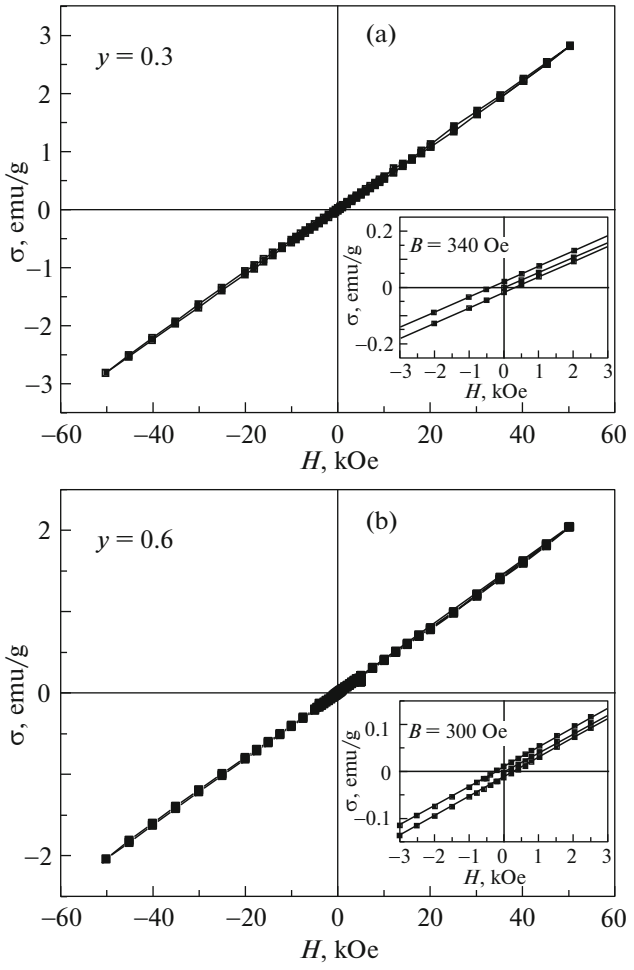

Fig. 6. Magnetic field dependences of magnetization σ for (a) $Sr_{0.8}Ce_{0.2}Mn_{0.7}Co_{0.3}O_{2.94}$ ($y = 0.3$) and (b) $Sr_{0.8}Ce_{0.2}Mn_{0.4}Co_{0.6}O_{2.69}$ ($y = 0.6$) at 2 K.

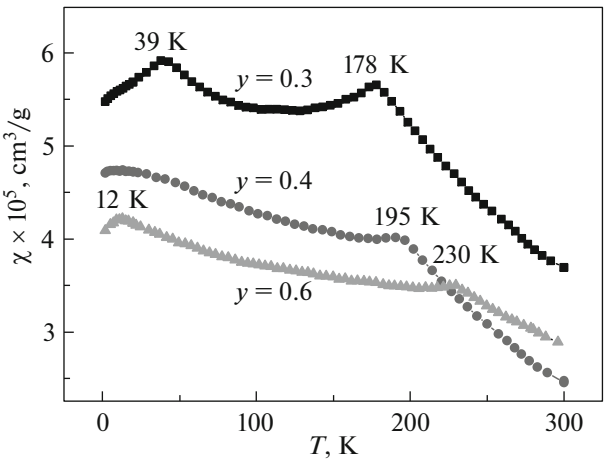

Fig. 7. Temperature dependence of ac magnetic susceptibility χ' for $Sr_{0.8}Ce_{0.2}Mn_{1-y}Co_yO_{3-\delta}$ at $y = 0.3$, 0.4, and 0.6.

Table 3. Experimental and calculated Mn and Co magnetic moments in the $Sr_{0.8}Ce_{0.2}Mn_{1-y}Co_yO_{3-\delta}$ solid solutions

y	Composition	μ_{calc}, μ_B	μ_{exp}, μ_B
0	$Sr_{0.8}Ce(IV_{0.2})Mn(IV_{0.6})Mn(III)_{0.4}O_3$	4.31	5.96 [8]
0.2	$Sr_{0.8}Ce_{0.2}Mn(IV)_{0.72}Mn(III)_{0.08}Co(II)_{0.02}O_{2.96}$	4.27	4.76
0.3	$Sr_{0.8}Ce_{0.2}Mn(IV)_{0.60}Mn(III)_{0.10}Co(II)_{0.20}Co(IIIHS)_{0.10}O_{2.94}$	4.38	4.40
0.4	$Sr_{0.8}Ce_{0.2}Mn(IV)_{0.60}Co(II)_{0.24}Co(IIIHS)_{0.04}Co(IIILS)_{0.12}O_{2.88}$	4.06	4.04
0.5	$Sr_{0.8}Ce_{0.2}Mn(IV)_{0.5}Co(II)_{0.25}Co(IIIHS)_{0.07}Co(IIILS)_{0.18}O_{2.75}$	3.99	3.96
0.6	$Sr_{0.8}Ce_{0.2}Mn(IV)_{0.40}Co(II)_{0.40}Co(IIIHS)_{0.07}Co(IIILS)_{0.20}O_{2.69}$	4.10	4.01

Mn^{4+}–Co^{2+} valence configuration, rather than Mn^{3+}–Co^{3+}, was also fixed. The μ_{exp} value higher than the calculated one can be attributed, as in $Sr_{0.8}Ce_{0.2}MnO_3$, to the formation of ferromagnetic clusters in the paramagnetic region.

As follows from Table 2, with a further increase in the Co content in the SS, the number of Mn^{3+} cations decreases (to 16% at $y = 0.3$) and, at $y = 0.4$ and 0.5, they completely vanish. As the oxygen content in these samples decreases, the bivalent cobalt content grows.

It is interesting to compare the examined Co and Mn valence state evolution with the available data on the $SrMn_{1-x}Co_xO_3$ system. In this system, in contrast to $Sr_{0.8}Ce_{0.2}Mn_{1-x}Co_xO_3$, the substitution of Co for Mn leads to the formation of a number of homologous compounds with the quasi-one-dimensional structure, including $Sr_{14}Mn_8Co_3O_{33}$, $Sr_9Mn_5Co_2O_{21}$, and $Sr_4Mn_2CoO_9$ [19]. In these compounds, the *d* elements are ordered in different structural positions in the form of Mn^{4+} and Co^{2+} cations. The presence of Mn^{4+} cations is considered to be the most probable situation in the $SrCo_{1-x}Mn_xO_{3-\delta}$ ($0 \le x \le 0.30$) SS [20]. It follows from Table 3 that in the $Sr_{0.8}Ce_{0.2}Mn_{1-y}Co_yO_3$ SS with increasing *y*, there is a trend to a decrease in the number of Mn^{3+} cations and preferred formation of the Mn^{4+}–Co^{2+} valence combination.

Based on the data from Table 3, we can explain the change in the unit cell parameters in the series of $Sr_{0.8}Ce_{0.2}Mn_{1-y}Co_yO_{3-\delta}$ (y = 0–0.6) SSs. The decrease in the tetragonal distortion and parameters *a* and *c* at the first stage is consistent with a decrease in the content of Jahn–Teller Mn^{3+} cations with an ionic radius of 0.645 Å [21], which are replaced by Co^{3+} cations with a smaller size (0.61 Å). Further, Co^{2+} cations with an ionic radius of 0.745 Å make a decisive contribution to the unit cell size and transition to the cubic structure.

To estimate the nature of the magnetic interactions in the investigated solid solutions, we used the data from [8, 9] that $Sr_{0.8}Ce_{0.2}MnO_3$ is characterized as a dilute antiferromagnet ($T_N = 210$ K) with a spin-glass-like state below 20 K and ferromagnetic clusters or a microscopic inhomogeneous magnetic phase in the paramagnetic region. Analysis of the Mn and Co valence and spin states in $Sr_{0.8}Ce_{0.2}Mn_{1-y}Co_yO_{3-\delta}$ (y = 0–0.6) on the basis of the magnetic measurements suggests that the possible antiferromagnetic (AFM) couplings in the investigated compositions are Mn^{3+}–O–Mn^{3+}, Mn^{4+}–O–Mn^{4+}, and Co^{3+}–O–Mn^{4+} and the ferromagnetic (FM) couplings are Co^{2+}–O–Mn^{4+} and Mn^{3+}–O–Mn^{4+}. In $Sr_{0.8}Ce_{0.2}MnO_3$, the magnetism is determined by the competition between the Mn^{3+}–O–Mn^{3+} and Mn^{4+}–O–Mn^{4+} couplings and the Mn^{3+}–O–Mn^{4+} couplings. The shift of the broad maximum in $Sr_{0.8}Ce_{0.2}Mn_{0.8}Co_{0.2}O_{2.95}$ to 138 K is indicative of the weakening of the short-range antiferromagnetic correlations at the retained complex $\chi^{-1}(T)$ dependence above this temperature. The positive constant Θ for this sample and a significant discrepancy between the ZFC and FC curves below 35 K point out the conservation of the competing ferromagnetic and antiferromagnetic couplings, which result in the spin-glass-like state at low temperatures. An increase in T_{max1} with the Co content (up to 239 K at $y = 0.6$) and the growth of the negative constant Θ are apparently due to the enhancement of the AFM Mn^{4+}–O–Mn^{4+} couplings against the background of the weakened FM couplings. The occurrence of a χ jump in the FC curve and a weak maximum in the ZFC $\chi(T)$ curve at 140 K in the $Sr_{0.8}Ce_{0.2}Mn_{0.4}Co_{0.6}O_2$ sample when measured in magnetic fields of 500 and 100 Oe evidence for the magnetic inhomogeneity of this sample and are caused by the high content of Co^{2+} cations and formation of FM Co^{2+}–Mn^{4+} clusters. This conclusion can be confirmed by the results of investigations of the $SrCo_{1-x}Mn_xO_{2.74}$ SS, in which the ferromagnetism with $T_C = 150$ K detected at the minimum Mn content (x = 0.05–0.10) is broken at the higher content of this element [20].

4. CONCLUSIONS

The results of crystal structure investigations and magnetic measurements of the electron-doped $Sr_{0.8}Ce_{0.2}Mn_{1-y}Co_yO_{3-\delta}$ (y = 0.2, 0.3, 0.4, 0.5, and 0.6) SSs allowed us to draw the following conclusions.

The solid solution with $y \geq 0.4$ undergoes a concentrational phase transition from the tetragonal syngony (sp. gr. $I4/mcm$) to the cubic one (sp. gr. $Pm3m$), which is stable up to $y = 0.7$. The observed structural transformation is related to the substitution of Co^{2+} and Co^{3+} cations for Jahn–Teller Mn^{3+} ions and a decrease in the oxygen content. The evolution of the magnetic properties of the SSs was analyzed using the available data on the $Sr_{0.8}Ce_{0.2}MnO_3$ manganite, which is characterized as a dilute antiferromagnet with $T_N = 250$ K and a spin-glass-like behavior and contains ferromagnetic clusters in the paramagnetic region at low temperatures. Upon the minimum substitution of cobalt for manganese ($y = 0.2$) in $Sr_{0.8}Ce_{0.2}MnO_3$, we observed a sharp decrease in T_N to 138 K, a positive Θ constant in the Curie–Weiss law, and a spin-glass-like behavior at $T < 35$ K. The behavior of the samples with the high cobalt content is caused by a further decrease in the content of Mn^{3+} cations (at $y = 0.3$) and their disappearance (at $y = 0.4$ and 0.5). As a result, the magnetic transformation point shifts to the high-temperature region, apparently due to the enhancement of the AFM Mn^{4+}–O–Mn^{4+} couplings at the retained spin-glass-like state at low temperature. In the sample with the maximum cobalt content, when measured in fields of 100 and 500 Oe, the region of ferromagnetic clusters was observed against the background of possible antiferromagnetism ($T_N = 230$ K) below 140 K.

REFERENCES

1. A. Urushibara, Y. Moritomo, T. Arima, A. Asamitsu, G. Kido, and Y. Tokura, Phys. Rev. B **51**, 14103 (1995).
2. M. Imada, A. Fujimori, and Y. Tokura, Rev. Mod. Phys. **70**, 1039 (1998).
3. S. Balamurugan, K. Yamaura, A. B. Karki, D. P. Young, M. Arai, and E. Takayama Muromachi, Phys. Rev. B **74**, 172406 (2006).
4. J. S. Srikiran, A. Das, P. L. Paulose, and S. K. Paranjpe, Appl. Phys. A **74**, S814 (2002).
5. N. Gayathri, A. K. Raychaudhuri, and S. K. Tiwary, Phys. Rev. B **56**, 1345 (1997).
6. G. V. Bazuev, A. V. Korolyov, M. A. Melkozyorova, and T. I. Chupakhina, J. Magn. Magn. Mater. **322**, 494 (2010).
7. A. Sundaresan, J. L. Tholence, A. Maignan, C. Martin, M. Hervieu, B. Raveau, and E. Suard, Eur. Phys. J. B **14**, 431 (2000).
8. W. J. Lu, B. C. Zhao, R. Ang, W. H. Song, J. J. Du, and Y. P. Sun, Phys. Lett. **346**, 321 (2005).
9. P. Mandal, A. Hassen, and A. Loidl, Phys. Rev. B **69**, 224418 (2004).
10. H. Gu, H. Chen, L. Gao, Y. Zheng, X. Zhu, and L. Guo, Electrochem. Acta **54**, 3532 (2009).
11. S. Balamurugan, K. Yamaura, M. Arai, and E. Takayama Muromachi, Phys. Rev. B **76**, 014414 (2007).
12. A. Maignan, B. Raveau, S. Hebert, V. Pralong, V. Caignaert, and D. Pelloquin, J. Phys.: Condens. Matter **18**, 4305 (2006).
13. P. D. Battle, T. C. Gibb, and C. W. Jones, J. Solid State Chem. **74**, 60 (1988).
14. H. Wu. K. Zhu, G. Xu, and H. Wang, Phys. B (Amsterdam, Neth.) **407**, 770 (2012).
15. Z. Zhang, C. J. Howard, D. Kennedy, M. Matsuda, and M. Miyake, J. Phys.: Condens. Matter **21**, 124218 (2009).
16. T. I. Chupakhina and G. V. Bazuev, Inorg. Mater. **47**, 1361 (2011).
17. S. N. Shamin, V. V. Mesilov, M. S. Udintseva, A. V. Korolev, T. I. Chupakhina, G. V. Bazuev, and V. R. Galakhov, Curr. Appl. Phys. **16**, 1597 (2016).
18. G. V. Bazuev and A. V. Korolyev, J. Magn. Magn. Mater. **320**, 2262 (2008).
19. G. V. Bazuev, Russ. Chem. Rev. **75**, 749 (2006).
20. A. Maignan, S. Hebert, N. Nguyen, V. Pralong, D. Pelloquin, and V. Caignaert, J. Magn. Magn. Mater. **303**, 197 (2006).
21. R. D. Shannon, Acta Crystallogr., A **32**, 75 (1976).

Translated by E. Bondareva